Heliyon 10 (2024) e37532

Contents lists available at ScienceDirect

Heliyon

journal homepage: www.cell.com/heliyon

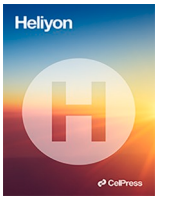

Research article

Transcriptomics and metabolomics revealed the molecular basis of the color formation in the roots of *Panax notoginseng*

Kang Ning [a,1], Hao Huai [a,b,1], Mengzhi Li [a], Yuli Xu [c], Fugang Wei [d], Zhongjian Chen [e], Yong Wang [e], Pengcheng Huang [c], Yuqi Yu [d], Shilin Chen [a], Linlin Dong [a,*]

[a] *Key Laboratory of Beijing for Identification and Safety Evaluation of Chinese Medicine, Institute of Chinese Materia Medica, China Academy of Chinese Medical Sciences, 100700, Beijing, China*
[b] *College of Biological & Pharmaceutical Sciences, China Three Gorges University, 443002, Yichang, China*
[c] *Zhangzhou Pianzaihuang Pharmaceutical Co., Ltd., 363099, Fujian, China*
[d] *Wenshan Miaoxiang Notoginseng Technology, Co., Ltd., 663000, Wenshan, China*
[e] *Institute of Sanqi Research, Wenshan University, 663000, Wenshan, China*

ARTICLE INFO

Keywords:
Panax notoginseng
Anthocyanin
Metabolome
Full-length transcriptome
R2R3-MYB

ABSTRACT

Panax notoginseng is a traditional Chinese medicine rich in many pharmacological components. The root of the 'Miaoxiang Sanqi No. 2' is yellow or greenish yellow, while a novel cultivar-'Wenyuan Ziqi No. 1' shows purple root and is thought to have high medicinal value. Little information is available about the anthocyanin biosynthesis in *P. notoginseng* root. In this study, we compared the 'Miaoxiang Sanqi No. 2' and 'Wenyuan Ziqi No. 1' in morphological, transcriptional and metabolic levels. The results showed that purple rich in the periderm, rhizome and phloem around cambium of the 'Wenyuan Ziqi No. 1' root and cyanidin 3-O-galactoside was the main anthocyanin causing purple. Moreover, 'Wenyuan Ziqi No. 1' highly accumulated in 155 metabolites, including flavones, phenylpropanoids and lipids. Transcriptome data showed that phenylpropanoid biosynthesis pathway genes are highly expressed in 'Wenyuan Ziqi No. 1'. Conjoint analysis showed that anthocyanin biosynthesis pathway substances were highly accumulated in 'Wenyuan Ziqi No. 1', and the expression level of structural genes involved in anthocyanin biosynthesis pathway was higher in 'Wenyuan Ziqi No. 1'. Meanwhile, eight *R2R3-MYB* genes that might be involved in anthocyanin biosynthesis were identified. The comprehensive analysis of two cultivars provides new insights into the understanding of root coloration in *P. notoginseng*.

1. Introduction

Panax notoginseng (Burk.) F. H. Chen(*P. notoginseng*) is a perennial herb that belongs to the Araliaceae family. The dried root of this

* Corresponding author.
E-mail addresses: cjdgtq@163.com (K. Ning), 15171443532@163.com (H. Huai), mengzhili0124@163.com (M. Li), yulixu2015@163.com (Y. Xu), weifugang@live.com (F. Wei), 18687656337@126.com (Z. Chen), ws-wangyong37@163.com (Y. Wang), hpc@zzpzh.com (P. Huang), yu-yu-qi@163.com (Y. Yu), slchen@icmm.ac.cn (S. Chen), lldong@icmm.ac.cn (L. Dong).
[1] These authors contributed equally to this work.

https://doi.org/10.1016/j.heliyon.2024.e37532
Received 17 June 2024; Received in revised form 27 August 2024; Accepted 4 September 2024
Available online 10 September 2024

plant, known as 'Sanchi', has been used as a Traditional Chinese Medicine for more than 2000 years [1]. *P. notoginseng* is rich in medicinal ingredients, including saponins, flavonoids, volatileoils, polysaccharides, and amino acids [2]. Based on bioactivity analyses, *P. notoginseng* has been shown to improve myocardial ischemia [3], defend against cardiovascular disease [4], lower blood pressure [5], and improve arteriosclerosis [6]. Many reports have demonstrated the antithrombotic and anticancer activities of *P. notoginseng* [7,8]. In addition, *P. notoginseng* is used in various prescriptions, and it has a wide market demand. The total annual output value of *P. notoginseng* can reach 70 billion RMB(Renminbi) [9].

Color is an important characteristic of plant. The color of plant organs is mainly attributed to flavonoids, chlorophylls, and carotenoids [10]. Anthocyanins, an important flavonoid, are widely distributed in flowers, fruits, and roots of plants, giving them various colors [11]. Up to now, more than 600 anthocyanins have been identified [12]. Pelargonidin, peonidin, delphinidin, cyanidin, petunidin and malvidin are the six common anthocyanins in plant [13]. Anthocyanins have various functions, such as attracting pollinator disperse seeds and improving plant resistance under biotic and abiotic stress conditions [14].

Flavonoids are produced from phenylalanine via the phenylpropanoid and flavonoid biosynthesis pathways. Flavonoid biosynthesis could be divided into two stages. In the early stage, phenylalanine is catalyzed by phenylalanine ammonia-lyase (PAL), cinnamic acid 4-hydroxylase (C4H), and 4 coumarate CoA ligase (4CL) to produce one 4-coumaroyl-CoA and three malonyl-CoA. These substances are subsequently catalyzed by chalcone synthase (CHS) and chalcone isomerase (CHI) to produce naringenin. Naringenin is a key intermediate substance in the process of flavonoid biosynthesis, it could be further catalyzed into dihydrokaempferol by flavanone 3-hydroxylase (F3H). In the later stage, dihydrokaempferol could be catalyzed into different types of flavonoids by a range of enzymes, such as flavonoid 3′-hydroxylase (F3′H), flavonoid 3′5′-hydroxylase (F3′5′H), dihydroflavonol 4-reductase (DFR), anthocyanidin synthase (ANS), and flavonol synthase (FLS). However, unstable anthocyanins need to be further glycosylated by UDP-glucose: flavonoid 3-O-glueosyltransferase (UFGT) to become stable anthocyanins before they could be transported and stored in cells [15–17].

Transcription factors (TFs) are highly involved in anthocyanin biosynthesis. Basic-helix-loop-helix (bHLH) and WD40 repeat (WD40) proteins interact with MYB to form MBW (MYB−bHLH−WD40) complex to regulate the accumulation of anthocyanin in many plants [18]. Other TFs were also reported to regulate anthocyanin biosynthesis. For example, SlMYB75 could improve the quality of tomato by increasing the content of anthocyanin [19]. MYB and HD-Zip could lead to the accumulation of anthocyanin in ripe jujube [20]. In *Arabidopsis thaliana*, MYB11, MYB12, MYB111, MYB113, MYB114, and TT2 could activate the expression of structural genes in anthocyanin biosynthesis [14,21,22]. MYBs are a group of TFs containing 1–4 MYB repeats. In accordance with the MYB repeat number, MYB proteins could be classified as MYB-related, R2R3-MYB, R1R2R3-MYB, and R4-MYB. R2R3-MYB TFs are involved in plant development, stress responses, and secondary metabolism, especially phenylpropanoid metabolism [23–25].

Several versions of *P. notoginseng* genome have been published, but some discontinuous and unknown regions still exist in the *P. notoginseng* genome [26–28]. RNA-seq could obtain the sequence and their expression profile, while next-generation sequencing (NGS), with only short sequencing reads (50–300 bp), requires fragmented transcripts for library construction. With the lack of high-quality genomic data as reference, NGS could lose important information, such as complete transcripts. The Pacific BioSciences (PacBio) sequencing platform, a single-molecule real time (SMRT) sequencing technology that reads the full length of cDNA, could efficiently obtain the whole sequence of a single RNA molecule with high quality [29].

P. notoginseng with purple root was first reported in 1999, and later researches showed that purple was caused by anthocyanin, *P. notoginseng* with purple root have advantages over the common *P. notoginseng* with yellow root in ecological adaptability and pharmacodynamic superiority [30]. On the one hand, anthocyanins have pharmacological activities similar to saponins, making anthocyanins have synergistic effects on the pharmacodynamics of *P. notoginseng*; on the other hand, anthocyanins have unique pharmacological activities that saponins do not have, making anthocyanins have complementary effects on the pharmacodynamics of *P. notoginseng* [30,31]. Therefore, *P. notoginseng* with purple root shows higher medicinal and economic value than the common *P. notoginseng* with yellow root [30]. In 2019, a novel cultivar- 'Wenyuan Ziqi No. 1' (No. 20190004) with purple root was bred. However, types and contents of metabolites and the molecular basis of anthocyanins biosynthesis in 'Wenyuan Ziqi No. 1' remains unknown.

Coloration is closely related to secondary metabolites, and it has an important effect on the quality of medicinal plants [32]. However, the reason for the formation of the purple in the root of *P. notoginseng* is currently elusive. Knowledge on the genetic basis of characters related to the quality of *P. notoginseng*, such as color formation, could facilitate their cultivation to obtain more economically valuable medicinal materials. With the further development and improvement of transcriptomics and metabolomics, joint analysis of the two omics has been extensively conducted to identify metabolites and related genes in medicinal plants [33,34]. Here, the phenotypic characters of two *P. notoginseng* cultivars (the 'Miaoxiang Sanqi No. 2' and the 'Wenyuan Ziqi No. 1') were observed. Liquid chromatography tandem mass spectrometry (LC-MS/MS) was used to detect the types and contents of anthocyanins. Combined analysis of metabolomics and transcriptomics was conducted to reveal the molecular basis of the color formation in the roots of *P. notoginseng*. This research provides valuable reference for the development and utilization of *P. notoginseng*.

2. Materials and methods

2.1. Plant materials

'Miaoxiang Sanqi No.2' (No. 20190003) and novel cultivar-'Wenyuan Ziqi No.1' (No. 20190004) were cultivated in Wenshan, Yunnan Province, China. 'Miaoxiang Sanqi No.2' is called the common *P. notoginseng* with yellow root (YR); 'Wenyuan Ziqi No.1' is called *P. notoginseng* with purple root (PR). In this study, two plant cultivars were selected that had been cultivated for three years. For both cultivars, the root tissue was thoroughly cleaned and cut into segments of appropriate size. The samples were then quickly frozen

in liquid nitrogen. After freezing, the samples were transferred to an ultra-low temperature refrigerator at −80 °C for long-term storage. These preserved samples will be used for subsequent metabolomics analysis, transcriptomic studies, and quantitative real-time polymerase chain reaction (qRT-PCR) experiments.

2.2. Identification and quantification of anthocyanins

After vacuum freeze-drying, the samples were ground into powder using a mixer mill (30 Hz, 1.5 min). The 50 mg powder was dissolved in 500 μL 80 % methanol aqueous solution (containing 0.1 % hydrochloric acid), and was repeatedly extracted by vortex (10 min), ultrasonic (10 min) and centrifugation (12,000 r/min, 3 min). Combined with supernatant, the supernatant was filtered through 0.22 μm PTFE microporous filter membrane and stored in the sample vial for LC-MS/MS analysis.

UPLC (ExionlC^{TM}AD) and MS/MS (QTRAP 6500+) were used for data acquisition. The chromatography was performed on ACQUITY BEH C18 column 1.7 μm, 2.1 mm*100 mm. The mobile phase A is ultra-pure water (containing 0.1 % formic acid) and B is methanol (containing 0.1 % formic acid). Elution gradient: 0.00min 5%B, 6.00min increased to 50%B, 12.00min increased to 95%B, held for 2 min, reduced to 5%B at 14 min, and balanced for 2 min. The flow rate was 0.35 mL/min, the column temperature was 40 °C, and the sample size was 2 μL. The mass spectrum conditions mainly include: Electrospray ion source (ESI) temperature 550 °C, mass spectrum voltage 5500 V in positive ion mode, Curtain Gas (CUR)35 psi.

A series of standard product solutions ranging from 0.01 to 5000 ng/mL were prepared, the peak intensity of mass spectrometry was measured, and the standard curve was drawn. The sample peak area is substituted into the standard curve equation to calculate the substance concentration.

The content of the detected substance in the sample (μg/g) = c × V/1000000/m.

The meaning of each letter in the formula: c: the concentration value obtained by substituting the integrated peak area in the sample into the standard curve (ng/mL); V: The volume of the solution used in redissolution (μL); m: Sample mass (g) taken.

2.3. Metabolomic profiling

The freeze-dried sample was pulverized using a mixer mill (MM 400, Retsch) and zirconia beads at 30 Hz for 1.5 min. Weigh 100 mg powder and extract it with 0.6 ml 70 % methanol solution at 4 °C overnight. After centrifugation of 10,000g for 10 min, the extract solution was passed through a CNWBOND Carbon-GCB SPE Cartridge (250 mg, 3 ml; ANPEL, Shanghai, China) was absorbed and used with 0.22 μm filter membrane (SCAA-104; ANPEL, Shanghai, China) was filtered and then analyzed by LC-MS.

The liquid chromatography was performed on Waters ACQUITY UPLC HSS T3 C18 column (1.8 μm diameter, 2.1 mm inner diameter × 100 mm length) with ultra-pure water (A phase) containing 0.04 % acetic acid and acetonitrile (B phase) containing 0.04 % acetic acid as mobile phases. The elution gradient starts from 5 % B phase at 0.00 min, increases linearly to 95 % B phase within 10.00 min and maintains for 1 min, then decreases to 5 % B phase within 0.00 min and completes equilibrium at 14.00 min. The experimental Settings included a flow rate of 0.35 mL/min, a column temperature of 40 °C, and an injection volume of 4 μL. The mass spectrum conditions mainly include:ESI temperature 550 °C, mass spectrum voltage 5500 V, CUR 30 psi. The quantitative monitoring mode for the metabolites was set to multiple reaction monitoring. DAMs between two cultivars were determined on the basis of the VIP $\geq$1 and fold change $\geq$2 or fold change $\leq$0.5.

2.4. RNA-Seq analysis

Samples were used to extract RNA. Total RNA was extracted with the Quick RNA Isolation Kit (Waryoung, China). A NanoDrop 2000 spectrophotometer and an Agilent 2100 Bioanalyzer were used to measure the total RNA concentration and quality. RNA samples that met the requirements were sent to Annoroad Gene Technology Co., Ltd (Beijing, China) for full-length transcriptome sequencing. In brief, The cDNA library was sequenced by the third generation sequencing platform of PacBio and the polymerase reads data were obtained. In turn, polymerase reads were filtered to remove low quality and short read length sequences. Then classification, clustering and correction are performed to obtain high-quality full-length sequences. These data were used for subsequent analysis. Plant transcription factors were predicted using Plant Transcription Factor Database (PlantTFDB). Coding-Non-Coding Index (CNCI), Coding Potential Calculator (CPC), and Coding Potential Assessment Tool (CPAT) were used for lncRNA analysis. The non-redundant transcripts were processed with COding GENome reconstruction Tool (Cogent version: 8.0.0, https://github.com/Magdoll/Cogent). Error-corrected non-redundant transcripts were mapped to UniTransModels using Genomic Mapping and Alignment Program (GMAP Version 2021-08-25, http://research-pub.gene.com/gmap/). AS events were identified by using SUPPA software (https://github.com/comprna/SUPPA).

High-quality consensus isoforms were used as the reference sequence, and the NGS data were compared with the reference sequence. The non-redundant transcript functions were annotated on the basis of the following databases: NR; NT; Pfam; KOG/COG; Swiss-Prot; GO; and KEGG. The Read Count of each isoform in each sample was quantified and the fragments per kilobase of transcript sequence per millions (FPKM) value was converted to obtain the gene expression level. Genes with $p \leq 0.05$, $|\log_2(\text{fold change})| \geq 0.6$ were identified as DEGs. GO and KEGG enrichment analyses of DEGs were further conducted [35–37].

2.5. Phylogenetic analysis

The full-length protein sequences of all *P. notoginseng* MYB family members identified in the transcriptome data along with 10

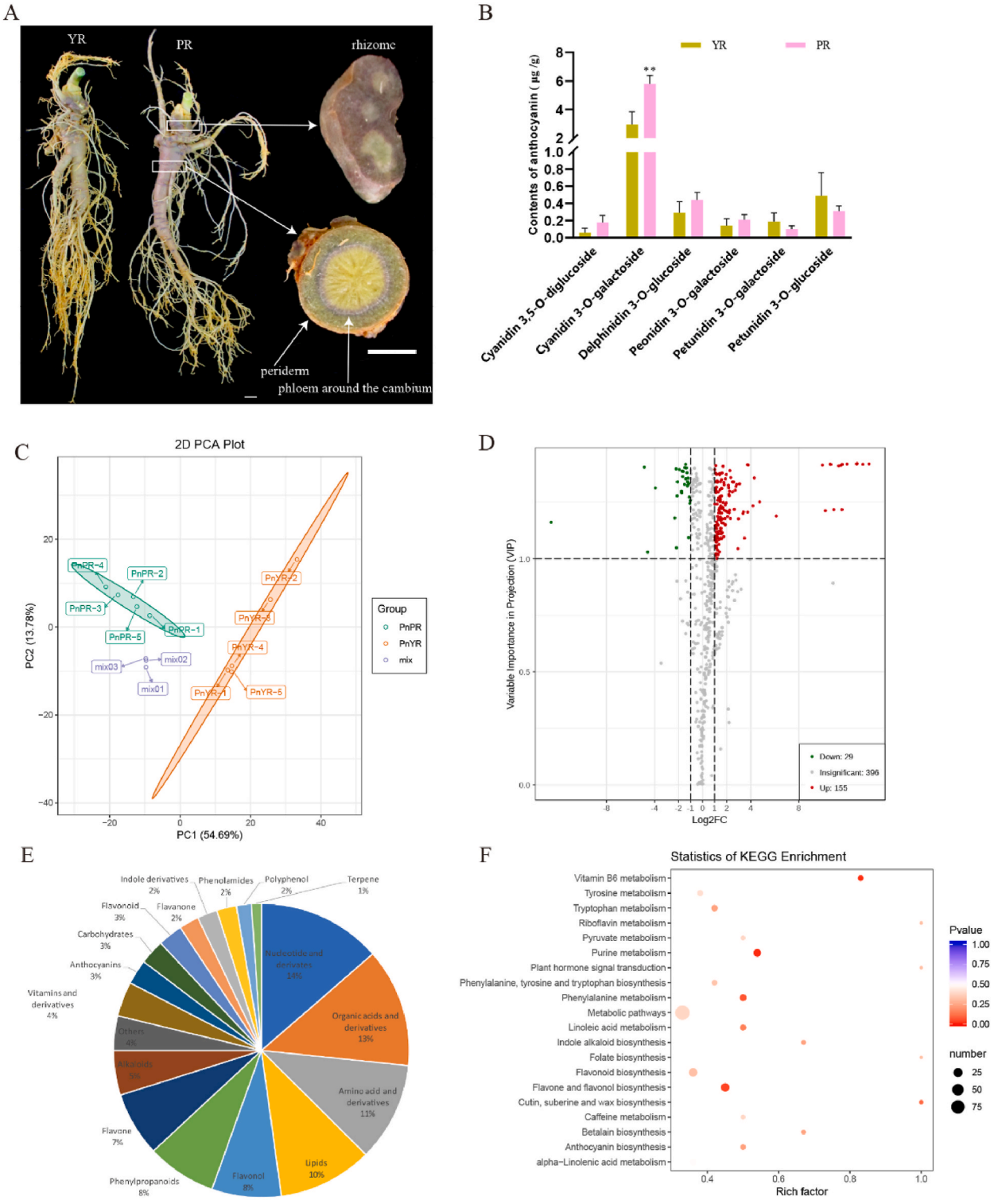

Fig. 1. Identification of anthocyanins and DAMs in the roots of two *P. notoginseng* cultivars. (A) Phenotypic characters of YR and PR. Scale bar = 1 cm. (B) Anthocyanin identification and quantification of YR and PR. Values are mean ± SD. *p < 0.05, **p < 0.01. (C) PCA of metabolites identified in YR and PR. (D) Volcano plots depicting the upregulated and downregulated DAMs in YR and PR. Up and down represent upregulated and downregulated DAMs, respectively. Insignificant represents nondifferentially accumulated metabolites. (E) Types and number of DAMs. (F) KEGG enrichment analysis of DAMs.

R2R3-MYB TFs (AaMYB2, CmMYB6, GmMYB10, GtMYB3, LhMYB12, MdMYBA, OgMYB1, PcMYB10, PeMYB2 and EsMYBA1) were used for phylogenetic analysis. Sequences were aligned with ClustalW, after which a phylogenetic tree was constructed according to the neighbor-joining method of the MEGA 7 program. The used sequences were listed in Table S1.

2.6. qRT-PCR analysis

The total RNA was extracted with the Quick RNA Isolation Kit (Waryoung, China), and cDNA was synthesized using the FastQuant RT Kit (Tiangen, China). Specific quantitative primers were designed by Primer 5.0, as listed in Table S2. *PnActin* gene used as an internal reference gene. qRT-PCR was performed using a TB Green Premix Ex Taq II kit (Takara, Dalian, China) on the SLAN-96P Real-time PCR system (SLAN, China). The reaction procedure was as follows: one cycle at 95 °C for 30 s; 40 cycles at 95 °C for 5 s; 60 °C for 30 s; and finally, 72 °C for 30 s. Gene expression levels were analyzed using the $2^{-\Delta\Delta Ct}$ method.

3. Result

3.1. Identification of anthocyanins and metabolome profiling in two P. notoginseng cultivars

Firstly, the phenotype of the two cultivars was observed. The root of 'Miaoxiang Sanqi No. 2' (the common *P. notoginseng* with yellow root, YR) was yellow or greenish yellow in appearance, while the root of 'Wenyuan Ziqi No. 1' (*P. notoginseng* with purple root, PR) was purple in appearance. Transection of the PR showed that the periderm, rhizome and phloem around the cambium were purple (Fig. 1A).

The types and contents of anthocyanins in YR and PR were analyzed using LC-MS/MS. The result showed that petunidin 3-O-galactoside and petunidin 3-O-glucoside were higher accumulated in YR than in PR. While, the contents of cyanidin 3,5-O-diglucoside, cyanidin 3-O-galactoside, delphinidin 3-O-glucoside, and peonidin 3-O-galactoside were higher in PR than in YR. And the content of cyanidin 3-O-galactoside was significantly highly accumulated in PR (Fig. 1B).

The widely targeted metabolomic approach was used to analyze the metabolites in the two cultivars and further explore the differences between them at the metabolite level. A total of 580 compounds, including 65 lipids, 43 phenylpropanoids, 35 flavones, 27 flavonols, 23 terpenes, and nine anthocyanins, were identified in the two cultivars (Table S3 and Fig. S1). Principal component analysis (PCA) of all the identified compounds showed that the two cultivars had a distinct difference at the metabolite level (Fig. 1C).

The differentially accumulated metabolites (DAMs) between the two cultivars were identified on the basis of VIP (variable importance in project) ≥ 1 and fold change ≥ 2 or fold change ≤ 0.5. In total, 184 DAMs were identified between the two cultivars, including 155 DAMs that were upregulated in PR and 29 DAMs that were upregulated in YR (Fig. 1D). The DAMs were mainly distributed in flavonoid compounds, including 13 flavones (7 %), 14 flavonols (8 %), five flavonoids (3 %), four flavanones (2 %) and five anthocyanins (3 %), followed by 25 nucleotides and derivatives (14 %), 24 organic acids and derivatives (13 %), 20 amino acids and derivatives (11 %), and 19 lipids (10 %) (Table S4 and Fig. 1E). For example, dihydromyricetin, phloretin, and tangeretin were highly accumulated in PR. KEGG (Kyoto Encyclopedia of Genes and Genomes) enrichment analysis showed that the DAMs were significant enriched in phenylalanine metabolism (ko00360) and flavone and flavonol biosynthesis (ko00944) pathways (Fig. 1F). Based on metabolomic data, five anthocyanins (delphinidin 3-O-glucoside, petunidin 3-O-glucoside, cyanidin, cyanidin O-acetylhexoside, and cyanidin 3-O-galactoside) were highly accumulated in PR (Table S4). Meanwhile, PR exhibited higher accumulation in flavones, flavonols, phenylpropanoids than YR.

3.2. Full-length transcriptomic analysis of two P. notoginseng cultivars

With the lack of high-quality *P. notoginseng* genome, the molecular basis of anthocyanin biosynthesis in *P. notoginseng* was investigated using full-length transcriptome. A total of 301,048 and 442,301 polymerase reads were obtained from YR and PR, respectively. The number of bases of polymerase reads from YR and PR were 17,808,549,065 and 21,584,822,325 bp, respectively (Table S5). Length distribution of polymerase reads was shown in Fig. S2. A total of 12,651,665 and 14,929,244 subreads were obtained from YR and PR, respectively. The number of bases of subreads from YR and PR were 17,259,214,056 and 20,935,756,761 bp, respectively (Table S6). Length distribution of subreads was shown in Fig. S3. For the YR, a total of 259,535 circular consensus sequencing (CCS) reads were generated, with a total of 380,771,821 bases. For the PR, a total of 364,758 CCS reads were generated, with a total of 545,489,649 bases (Table S7). A total of 259,535 and 364,758 reads of insert (ROIs) were obtained from YR and PR,

Table 1
Summary of consensus isoforms in the roots of two *P. notoginseng* cultivars.

Sample	YR	PR
Number of Consensus Isoforms	231,046	316,477
Mean Length of Consensus Isoforms	1344.38	1369.94
Number of High-quality Isoforms	19,840	27,019
Mean Length of High-quality Isoforms	1406.12	1417.23
Number of Low-quality Isoforms	7	33
Mean Length of Low-quality Isoforms	1354.14	1673.85

respectively, and the mean lengths of the ROIs from YR and PR were 1467.13 and 1495.48 bp, respectively. The GC% of YR and PR were 42.25 % and 42.30 %, respectively (Table S8). After consensus isoforms were clustered and corrected, 19,840 and 27,019 high-quality isoforms were obtained from YR and PR, respectively. The mean lengths of the high-quality isoforms from YR and PR were 1406.12 and 1417.23 bp, respectively (Table 1). Length distribution of consensus isoforms is shown in Fig. S4.

Totally, 19,728 and 27,193 ORFs were identified in YR and PR, respectively (Table S9), length distribution of ORFs was shown in Fig. S5. 9336 genes were successfully annotated in four databases(Fig. S6a). Nearly 60 % genes were involved in metabolic process, and 49 % genes showed catalytic activity in molecular function (Fig. S6b). Furthermore, 63 % genes were annotated in the metabolism group in KEGG database (Fig. S6c). and a large proportion of genes was allocated to 'posttranslational modification, protein turnover, chaperones' and 'secondary metabolite biosynthesis, transport, and catabolism' (Fig. S6d).

A total of 8279 and 11345 putative TF genes were identified in the YR and PR, respectively (Table S10). Among all TF families, the bHLH family was the largest group in both YR and PR (822, 9.93 % in YR and 1106, 9.75 % in PR). B3, MYB-related, ERF and NAC TF families were detected in the two cultivars (Fig. S7 and Table S10). It suggested that transcriptional regulation was active in the root of *P. notoginseng.* In addition, 984 and 1279 candidate long non-coding RNAs (lncRNAs) were predicted in the YR and PR, respectively. The length distribution of lncRNAs was shown in Fig. S8.

One advantage of PacBio Iso-Seq is its ability to describe the complexity of alternative splicing (AS) at the whole-transcriptome scale. In YR, 5404 full-length unique transcript models (UniTransModels) were obtained and 38.43 % of these had more than one isoform. While, 6874 UniTransModels were obtained in PR, of which 42.12 % had more than one isoform (Fig. 2A). Then we identified AS events in two cultivars and 91 and 122 AS events were identified in YR and PR, respectively (Fig. 2B). UniTransModel-based retained introns (RI) were identified as the most abundant AS event in both YR and PR. Together with alternative 5′ splice-site (A5) and alternative 3′ splice-site (A3) AS events, these three types of AS event accounted for >90 % of detected AS events (Fig. 2B). An UniTransModel can produce many different splicing isoforms through AS events. Gene that encodes 4-coumarate-CoA ligase-like 5 protein (PB.4079, LOC102606631) can produce seven different splicing isoforms in YR. While, gene that encodes auxilin-like protein 1(PB.1160, LOC105633821) can produce four different splicing isoforms in PR (Fig. 2C).

PCA showed that two cultivars have a distinct difference in transcriptional level (Fig. 3A). A total of 2091 differentially expressed genes (DEGs) ($p \leq 0.05$, $|\log_2 (\text{fold change})| \geq 0.6$) were identified in transcriptome. 1181 DEGs were up-regulated in PR, 910 DEGs were highly expressed in YR. (Fig. 3B). In PR, KEGG analysis indicated that DEGs were enriched in phenylpropanoid biosynthesis

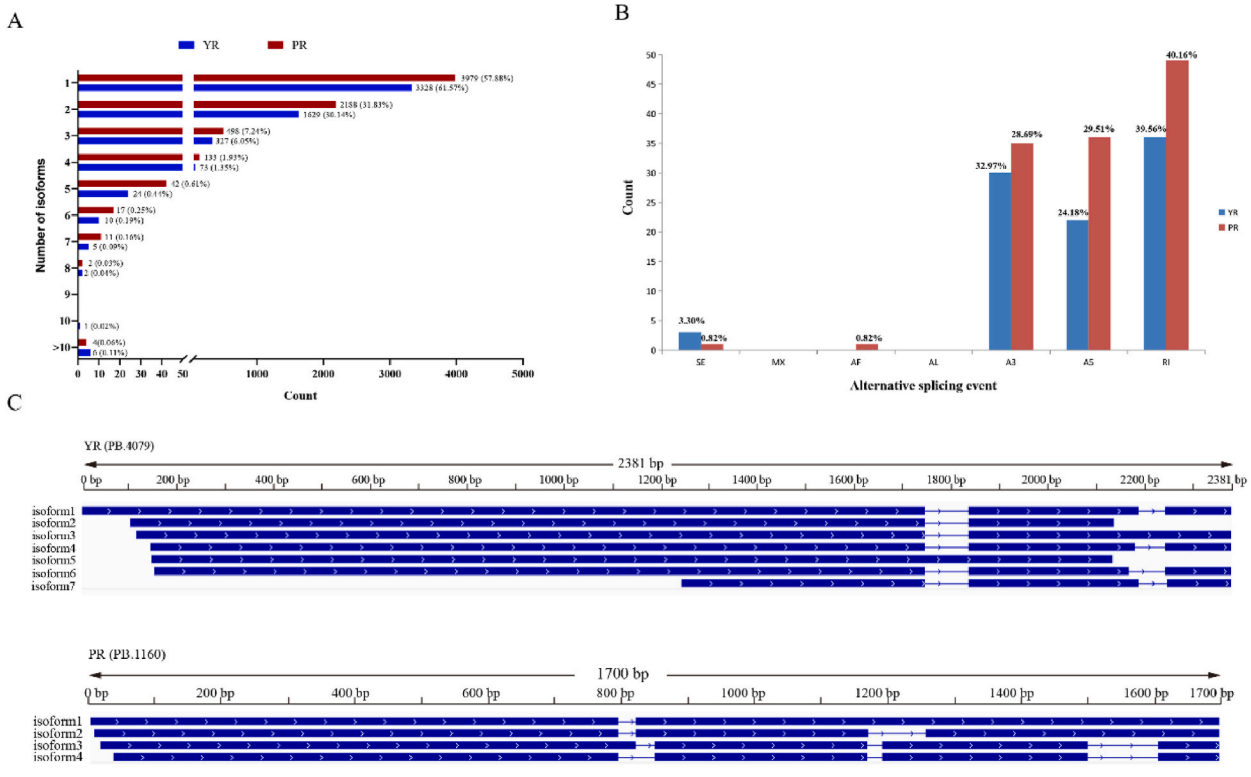

Fig. 2. Isoform analysis of *P. notoginseng* full-length transcriptomes using Iso-Seq. (A) Distribution of isoform numbers for UniTransModels in YR and PR. (B) Numbers of different AS events detected in full-length transcriptomes from YR and PR. SE, skipping exon; MX, mutually exclusive exon; AF, alternative first exon; AL, alternative last exon; A3, alternative 3′ splice-site; A5, alternative 5′ splice-site; RI, retained intron. (C) isoforms of different gene in YR and PR. PB.4079 represents the gene encoding 4-coumarate–CoA ligase-like 5 protein (Gene symbol:LOC102606631); PB.1160 represents the gene encoding auxilin-like protein 1 (Gene symbol: LOC105633821).

(map00940) pathway (Fig. 3C). In YR, KEGG analysis indicated that DEGs were enriched in flavonoid biosynthesis (map00941) pathway (Fig. 3D).

3.3. Transcriptomic and metabolomic analysis of anthocyanin biosynthesis pathway

This study then focused on the anthocyanin biosynthesis pathway. Anthocyanins (cyanidin and delphinidin) were highly accumulated in PR. Naringin, a key metabolite in the pathway, was also more highly accumulated in PR than in YR (Table S3). The expression levels of the structural genes involved in anthocyanin biosynthesis pathway were also detected. Six genes (*PnPAL1*, *PnPAL2*, *Pn4CL1*, *Pn4CL2*, *Pn4CL3* and *PnF3H3*) were upregulated in PR, while seven genes (*PnCHI*, *PnF3H1*, *PnF3H2*, *PnF3′H1*, *PnF3′H2*, *PnF3′5′H* and *PnUFGT*) were downregulated in PR (Fig. 4A). Pearson correlation analysis showed that the contents of most metabolites in the anthocyanin biosynthesis pathway were positively correlated with the expression levels of these six upregulated genes (Fig. S9). The cyanidin and delphinidin derivatives are purple pigment [38], and the contents of cyanidin 3-O-galactside and delphinidin 3-O-glucoside were higher in PR than in YR. Correlation analysis showed that the contents of cyanidin 3-O-galactoside and delphinidin 3-O-glucoside were positively correlated with the expression levels of these six upregulated genes (Fig. 4B). Furthermore, we also

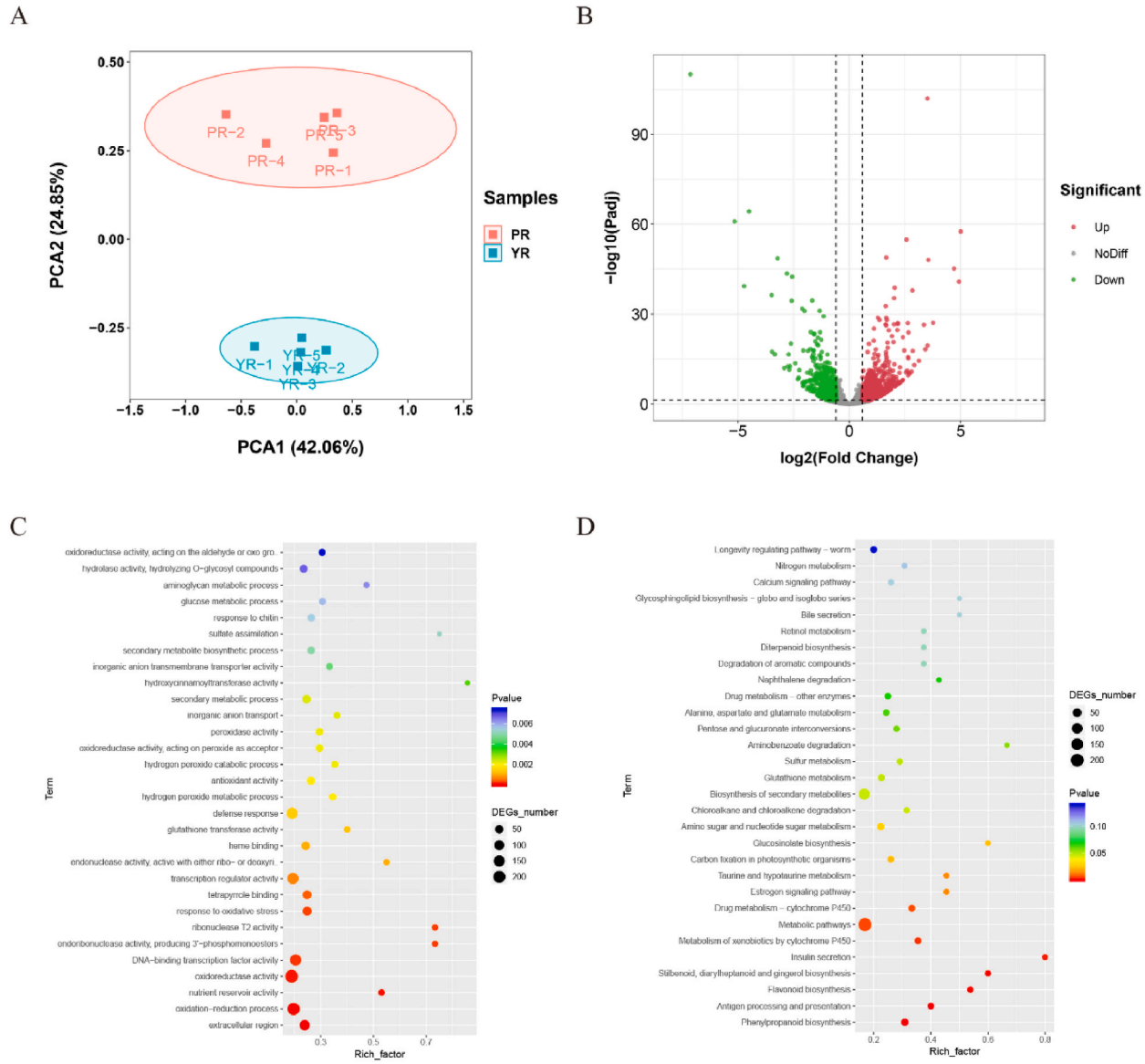

Fig. 3. DEGs and KEGG enrichment analysis of YR and PR. (A) PCA of genes identified in YR and PR. (B) Volcano plots displaying the upregulated DEGs in PR and YR. No Diff represents nondifferentially expressed genes. (C) KEGG enrichment analysis of upregulated DEGs in PR. (D) KEGG enrichment analysis of upregulated DEGs in YR.

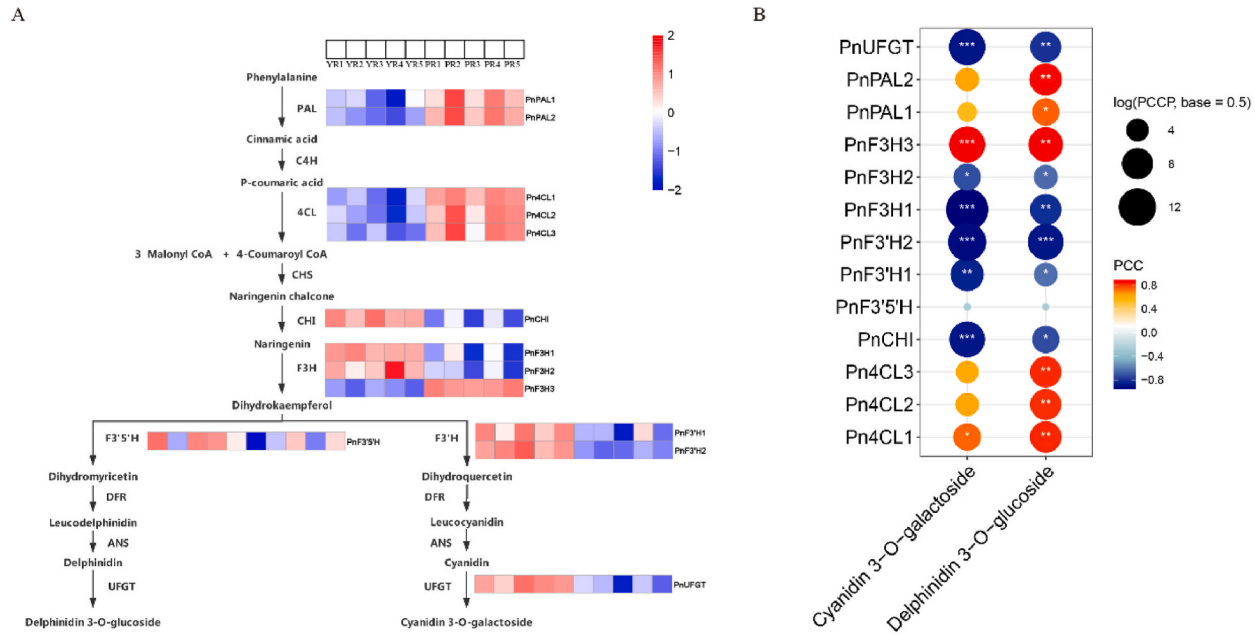

Fig. 4. Conjoint analysis of genes and metabolites related to anthocyanin biosynthesis in *P. notoginseng*. (A) Expression profiles of DEGs from the anthocyanin biosynthesis pathway in *P. notoginseng*. The color scale from blue (low) to red (high) represents the FPKM values measured in *P. notoginseng*. Enzymes in the pathway are shown as follows: phenylalanine ammonia-lyase (PAL), cinnamic acid 4-hydroxylase (C4H), 4 coumarate CoA ligase (4CL), chalcone synthase (CHS), chalcone isomerase (CHI), flavanone 3-hydroxylase (F3H), flavonoid 3′-hydroxylase (F3′H), flavonoid 3′,5′-hydroxylase (F3′5′H), dihydroflavonol 4-reductase (DFR), anthocyanidin synthase (ANS), and UDP-flavonoid glucosyl transferase (UFGT). (B) Pearson correlation analysis between the expression of DEGs and the content of cyanidin 3-O-galactoside and delphinidin 3-O-glucoside. The color scale from blue (low) to red (high) represents the level of Pearson correlation coefficient.

identified that one gene involved in anthocyanin biosynthesis pathway had AS events in PR, *UFGT* gene, PB.168. whereas no genes were found that had AS events in anthocyanin biosynthesis pathway in YR (Fig. S10). Our full-length Iso-Seq transcriptome can provide additional information for characterization of the anthocyanin biosynthesis pathway at a deeper transcription isoform level in *P. notoginseng*.

3.4. Identification of TFs related to anthocyanin biosynthesis in P. notoginseng

R2R3 MYB TFs were thought to regulate anthocyanin biosynthesis in plants. A total of 116 MYB TF genes, 85 *bHLH* TF genes, and 8 *WD40* TF genes were identified, and they showed different expression patterns in YR and PR (Fig. S11). In addition, the full-length protein sequences of 116 *P. notoginseng* MYB TFs and 10 R2R3 MYB TFs (AaMYB2, CmMYB6, GmMYB10, GtMYB3, LhMYB12, MdMYBA, OgMYB1, PcMYB10, PeMYB2 and EsMYBA1) were used to construct phylogenetic tree. The result showed that 12 *P. notoginseng* MYB TFs were clustered with the 10 R2R3 MYB TFs (Fig. 5A). Multi-sequence alignment showed that these genes contain the R2 and R3 domain (Fig. 5B). Then, the expression of genes was detected in YR and PR. *PnMYB1*, *PnMYB4*, *PnMYB5*, *PnMYB7*, *PnMYB33*, *PnMYB55*, *PnMYB67* and *PnMYB76* were highly expressed in PR (Fig. 5C), suggesting that these TFs may be involved in the regulation of anthocyanin biosynthesis in *P. notoginseng*.

3.5. Verification of RNA-seq results by qRT-PCR

Five DEGs from RNA-seq data were identified, and qRT-PCR analysis was performed on them to verify the reliability of transcriptomic data. The results showed that the expression in qRT-PCR was consistent with that in RNA-seq results (Fig. S12), proving that the transcriptomic data were reliable.

4. Discussion

P. notoginseng is a traditional Chinese herbal medicinal plant containing abundant active metabolites that beneficial to human health [39]. In this study, 580 compounds belonging to 22 classes were identified in metabolome. Many lipids, phenylpropanoids, flavones, alkaloids, and terpenes were detected in *P. notoginseng* root, suggesting that these substances may also play an important role in medicines or healthcare products containing *P. notoginseng*.

Anthocyanins have multifunction in plants, including protective function against biotic and abiotic stresses [40]. What's more,

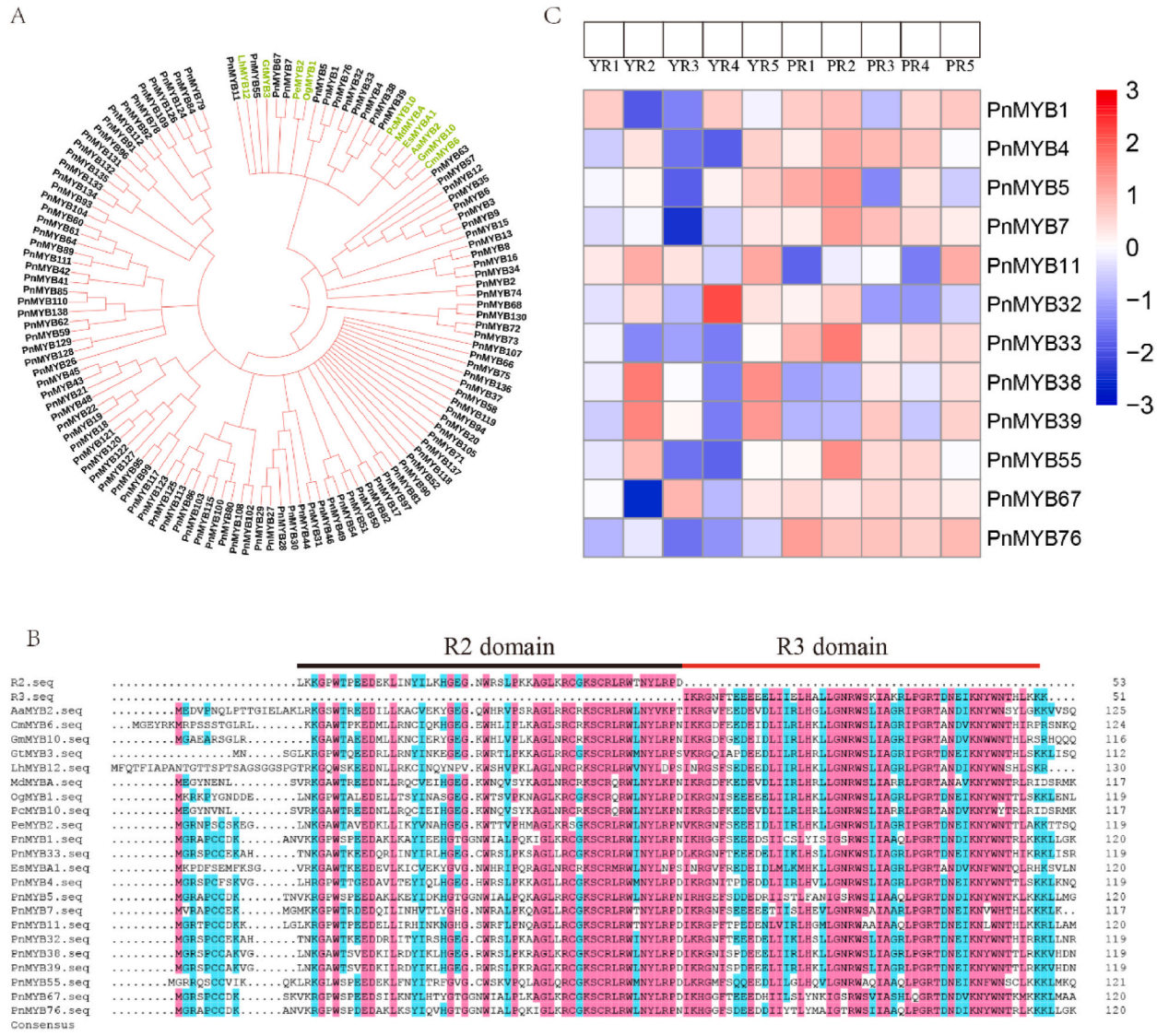

Fig. 5. Identification of MYB TF related to anthocyanin biosynthesis. (A) Phylogenetic tree of MYB TF. (B) Multiple alignments of amino acid sequences of 12 *P. notoginseng* MYB TFs with the 10 R2R3-MYB TFs. The black and red line represent the R2 and R3 domain, respectively. (C) Expression levels of 12 *R2R3-MYB* TF genes.

eating anthocyanin-rich food is beneficial for human health because anthocyanins are health-promoting compounds due to their antioxidant activity, anti-aging activity, and the ability to cut down the risk of cancers and diabetes [41,42]. Meanwhile, a high content of anthocyanins in edible organs and tissues is usually correlated with high quality. For example, purple wheat cultivars with a higher content of total phenolics, flavonoids, and anthocyanins than white wheat cultivars have been developed as valuable germplasms in breeding programs [43]. The quality of red longan is superior to that of yellow-brown longan because it contains more anthocyanins, flavonoids and flavonols [32]. *P. notoginseng* with purple root has more advantage in pharmacodynamics than the common *P. notoginseng* with yellow root [30]. Metabolome data showed that 155 metabolites including anthocyanins, flavonoids and terpenes are highly accumulated in PR than YR (Table S4). Therefore, PR has higher medicinal value and should be further promoted.

P. notoginseng with purple root showed higher medicinal value, but mechanism of anthocyanin biosynthesis is rarely studied in *P. notoginseng*. By comparing two cultivars in morphological, transcriptional and metabolomics level, our study provides abundant information for the further study of anthocyanin biosynthesis in *P. notoginseng*. 1) Anthocyanins were mainly distributed in the periderm, rhizome and phloem around cambium of the novel cultivar-'Wenyuan Ziqi No. 1' root (Fig. 1A). Cyanidin derivatives were water-soluble plant pigments that endow plant organs and tissues with purple appearance [16], such as jujube leaf [44], sweet potatoes [45] and radish [46]. Cyanidin, cyanidin O-acetylhexoside and cyanidin 3-O-galactoside especially cyanidin 3-O-galactoside were the main anthocyanins causing purple root in *P. notoginseng*. In addition, the substances in the anthocyanin biosynthesis pathway, namely, D-(+)-phenylalanine (pmf0594), naringin (pme0330), and dihydroquercetin (pme1521), were also highly accumulated in PR than in

YR (Table S3). 2) Lacking of high-quality genome data, we preformed full-length transcriptome and next-generation transcriptome to analyze the transcriptional difference between two cultivars. Lots of DEGs were identified between two cultivars and they were enriched in different metabolic pathways. DEGs that highly expressed in PR were enriched in phenylpropanoid biosynthesis (map00940) pathway. 3) Joint analysis of transcriptome and metabolome showed that metabolites involved in anthocyanin biosynthesis pathway were highly accumulated in PR. Meanwhile, six structural genes (*PnPAL1*, *PnPAL2*, *Pn4CL1*, *Pn4CL2*, *Pn4CL3* and *PnF3H3*) involved in anthocyanin biosynthesis were highly expressed in PR (Fig. 4A), and positively correlated with contents of cyanidin 3-O-galactoside and delphinidin 3-O-glucoside (Fig. 4B). It suggested that these genes may be important structural genes regulating the biosynthesis of *P. notoginseng* anthocyanin. Thus, our data suggested that high expression level of these six structural genes caused the high level of anthocyanins especially the cyanidin 3-O-galactoside, leading to the purple of the *P. notoginseng*.

Meanwhile, there are several speculations about anthocyanin biosynthesis in *P. notoginseng* generate from our study.

1) R2R3-MYB TFs play important role in anthocyanin biosynthesis by regulating the expression of structural genes [47]. 12 *R2R3-MYB* genes were identified in the transcriptome data and eight of which (*PnMYB1*, *PnMYB4*, *PnMYB5*, *PnMYB7*, *PnMYB33*, *PnMYB55*, *PnMYB67* and *PnMYB76*) were highly expressed in PR. Meanwhile, several MYB binding cis-elements were found in the promoter of the *PnPAL1*, *PnPAL2 and Pn4CL1* (Fig. S13). These R2R3-MYB TFs may regulate anthocyanin biosynthesis by binding to the promoter of the structure genes.
2) lncRNAs play important roles in regulating various biological processes including growth and stress responses in plants [48]. In our study, a large number of lncRNAs were identified in two *P. notoginseng* cultivars and these lncRNAs might play important roles in the biological process in *P. notoginseng*.
3) Alternative splicing was widely existed in *P. notoginseng* and we found that the alternative splicing level in the PR is higher than that in the YR (Fig. 2B). UFGT activity is positively associated with anthocyanin enrichment [49], and alternative splicing events were found in the *UFGT* gene. Thus, alternative splicing might also involve in anthocyanin biosynthesis in *P. notoginseng*.

5. Conclusions

In summary, we compared the 'Miaoxiang Sanqi No.2' and the 'Wenyuan Ziqi No.1' in morphological, transcriptional and metabolic levels. We found that anthocyanin, mainly cyanidin 3-O-galactoside, rich in the periderm, rhizome and phloem around cambium of the 'Wenyuan Ziqi No.1' root. Moreover, 155 metabolites were highly accumulated in 'Wenyuan Ziqi No.1'. Conjoint analysis showed that anthocyanin biosynthesis pathway substances were highly accumulated in 'Wenyuan Ziqi No.1', and structural genes involved in anthocyanin biosynthesis pathway were also highly expressed in 'Wenyuan Ziqi No.1'. Meanwhile, eight *R2R3-MYB* genes that might be involved in anthocyanin biosynthesis were identified. The comprehensive analysis of two cultivars provides new insights into the understanding of root coloration in *P. notoginseng*.

Funding

This study was supported by grants from the National Key R&D Plan (No. 2022YFC3501804), Fundamental Research Funds for the Central public welfare research institutes (No. ZZ13-YQ-049 and ZXKT22001), Scientific Research Project of Hainan Academician Innovation Platform (No. YSPTZX202137).

Data availability statement

Raw data of transcriptome are available in National Genomics Data Center (NGDC) under accession number PRJCA005818.

CRediT authorship contribution statement

Kang Ning: Writing – original draft. **Hao Huai:** Writing – original draft. **Mengzhi Li:** Methodology. **Yuli Xu:** Resources. **Fugang Wei:** Resources. **Zhongjian Chen:** Resources. **Yong Wang:** Resources. **Pengcheng Huang:** Resources. **Yuqi Yu:** Resources. **Shilin Chen:** Writing – review & editing. **Linlin Dong:** Writing – review & editing.

Declaration of competing interest

The authors declare that they have no known competing financial interests or personal relationships that could have appeared to influence the work reported in this paper.

Appendix A. Supplementary data

Supplementary data to this article can be found online at https://doi.org/10.1016/j.heliyon.2024.e37532.

References

[1] D. Zhang, W. Li, E.H. Xia, et al., The medicinal herb *Panax notoginseng* genome provides insights into ginsenoside biosynthesis and genome evolution, Mol. Plant 10 (6) (2017) 903–907, https://doi.org/10.1016/j.molp.2017.02.011.

[2] L. Jia, T. Zuo, C. Zhang, et al., Simultaneous profiling and holistic comparison of the metabolomes among the flower buds of *Panax ginseng, Panax quinquefolius*, and *Panax notoginseng* by UHPLC/IM-QTOF-HDMS(E)-based metabolomics analysis, Molecules 24 (11) (2019), https://doi.org/10.3390/molecules24112188.

[3] E.Y. Zhang, B. Gao, H.L. Shi, et al., 20(S)-protopanaxadiol enhances angiogenesis via HIF-1α-mediated VEGF secretion by activating p70S6 kinase and benefits wound healing in genetically diabetic mice, Exp. Mol. Med. 49 (10) (2017) e387, https://doi.org/10.1038/emm.2017.151.

[4] H. Liu, X. Lu, Y. Hu, X. Fan, Chemical constituents of *Panax ginseng* and *Panax notoginseng* explain why they differ in therapeutic efficacy, Pharmacol. Res. 161 (2020) 105263, https://doi.org/10.1016/j.phrs.2020.105263.

[5] C. Pan, Y. Huo, X. An, et al., *Panax notoginseng* and its components decreased hypertension via stimulation of endothelial-dependent vessel dilatation, Vasc. Pharmacol. 56 (3–4) (2012) 150–158, https://doi.org/10.1016/j.vph.2011.12.006.

[6] Y. Liu, F. Hao, H. Zhang, D. Cao, X. Lu, X. Li, *Panax notoginseng* saponins promote endothelial progenitor cell mobilization and attenuate atherosclerotic lesions in apolipoprotein E knockout mice, Cell. Physiol. Biochem. 32 (4) (2013) 814–826, https://doi.org/10.1159/000354484.

[7] X. Dang, J.J. Miao, A.Q. Chen, et al., The antithrombotic effect of RSNK in blood-stasis model rats, J. Ethnopharmacol. 173 (2015) 266–272, https://doi.org/10.1016/j.jep.2015.06.030.

[8] C.Y. Lee, S.L. Hsieh, S. Hsieh, et al., Inhibition of human colorectal cancer metastasis by notoginsenoside R1, an important compound from *Panax notoginseng*, Oncol. Rep. 37 (1) (2017) 399–407, https://doi.org/10.3892/or.2016.5222.

[9] Z. Jiang, L. Tu, W. Yang, et al., The chromosome-level reference genome assembly for *Panax notoginseng* and insights into ginsenoside biosynthesis, Plant Commun 2 (1) (2021) 100113, https://doi.org/10.1016/j.xplc.2020.100113.

[10] H.N. Zhang, W.C. Li, H.C. Wang, et al., Transcriptome profiling of light-regulated anthocyanin biosynthesis in the pericarp of litchi, Front. Plant Sci. 7 (2016) 963, https://doi.org/10.3389/fpls.2016.00963.

[11] Q. Shi, J. Du, D. Zhu, X. Li, X. Li, Metabolomic and transcriptomic analyses of anthocyanin biosynthesis mechanisms in the color mutant *ziziphus jujuba* cv, Tailihong, J. Agric. Food Chem. 68 (51) (2020) 15186–15198, https://doi.org/10.1021/acs.jafc.0c05334.

[12] J. He, M.M. Giusti, Anthocyanins: natural colorants with health-promoting properties, Annu. Rev. Food Sci. Technol. 1 (2010) 163–187, https://doi.org/10.1146/annurev.food.080708.100754.

[13] L. Jaakola, New insights into the regulation of anthocyanin biosynthesis in fruits, Trends Plant Sci. 18 (9) (2013) 477–483, https://doi.org/10.1016/j.tplants.2013.06.003.

[14] W. Xu, C. Dubos, L. Lepiniec, Transcriptional control of flavonoid biosynthesis by MYB-BHLH-WDR complexes, Trends Plant Sci. 20 (3) (2015) 176–185, https://doi.org/10.1016/j.tplants.2014.12.001.

[15] T. Jiang, M. Zhang, C. Wen, et al., Integrated metabolomic and transcriptomic analysis of the anthocyanin regulatory networks in *Salvia miltiorrhiza* Bge. flowers, BMC Plant Biol. 20 (1) (2020) 349, https://doi.org/10.1186/s12870-020-02553-7.

[16] Y. Liu, J. Lv, Z. Liu, et al., Integrative analysis of metabolome and transcriptome reveals the mechanism of color formation in pepper fruit (*Capsicum annuum* L.), Food Chem. 306 (2020) 125629, https://doi.org/10.1016/j.foodchem.2019.125629.

[17] Y. Xia, W. Chen, W. Xiang, et al., Integrated metabolic profiling and transcriptome analysis of pigment accumulation in *Lonicera japonica* flower petals during colour-transition, BMC Plant Biol. 21 (1) (2021) 98, https://doi.org/10.1186/s12870-021-02877-y.

[18] S. Bai, R. Tao, L. Yin, et al., Two B-box proteins, PpBBX18 and PpBBX21, antagonistically regulate anthocyanin biosynthesis via competitive association with *Pyrus pyrifolia* ELONGATED HYPOCOTYL 5 in the peel of pear fruit, Plant J. 100 (6) (2019) 1208–1223, https://doi.org/10.1111/tpj.14510.

[19] W. Jian, H. Cao, S. Yuan, et al., SlMYB75, an MYB-type transcription factor, promotes anthocyanin accumulation and enhances volatile aroma production in tomato fruits, Hortic. Res. 6 (2019) 22, https://doi.org/10.1038/s41438-018-0098-y.

[20] Q. Zhang, L. Wang, Z. Liu, et al., Transcriptome and metabolome profiling unveil the mechanisms of *Ziziphus jujuba* Mill. peel coloration, Food Chem. 312 (2020) 125903, https://doi.org/10.1016/j.foodchem.2019.125903.

[21] F. Mehrtens, H. Kranz, P. Bednarek, B. Weisshaar, The Arabidopsis transcription factor MYB12 is a flavonol-specific regulator of phenylpropanoid biosynthesis, Plant Physiol 138 (2) (2005) 1083–1096, https://doi.org/10.1104/pp.104.058032.

[22] R. Stracke, H. Ishihara, G. Huep, et al., Differential regulation of closely related R2R3-MYB transcription factors controls flavonol accumulation in different parts of the *Arabidopsis thaliana* seedling, Plant J. 50 (4) (2007) 660–677, https://doi.org/10.1111/j.1365-313X.2007.03078.x.

[23] I. Romero, A. Fuertes, M.J. Benito, J.M. Malpica, A. Leyva, J. Paz-Ares, More than 80 R2R3-MYB regulatory genes in the genome of *Arabidopsis thaliana*, Plant J. 14 (3) (1998) 273–284, https://doi.org/10.1046/j.1365-313x.1998.00113.x.

[24] R. Stracke, M. Werber, B. Weisshaar, The R2R3-MYB gene family in *Arabidopsis thaliana*, Curr. Opin. Plant Biol. 4 (5) (2001) 447–456, https://doi.org/10.1016/s1369-5266(00)00199-0.

[25] C.K. Jiang, G.Y. Rao, Insights into the diversification and evolution of R2R3-MYB transcription factors in plants, Plant Physiol 183 (2) (2020) 637–655, https://doi.org/10.1104/pp.19.01082.

[26] W. Chen, L. Kui, G. Zhang, et al., Whole-genome sequencing and analysis of the Chinese herbal plant *Panax notoginseng*, Mol. Plant 10 (6) (2017) 899–902, https://doi.org/10.1016/j.molp.2017.02.010.

[27] G. Fan, X. Liu, S. Sun, et al., The chromosome level genome and genome-wide association study for the agronomic traits of *Panax notoginseng*, iScience 23 (9) (2020) 101538, https://doi.org/10.1016/j.isci.2020.101538.

[28] Z. Yang, G. Liu, G. Zhang, et al., The chromosome-scale high-quality genome assembly of *Panax notoginseng* provides insight into dencichine biosynthesis, Plant Biotechnol. J. 19 (5) (2021) 869–871, https://doi.org/10.1111/pbi.13558.

[29] T. Wang, H. Wang, D. Cai, et al., Comprehensive profiling of rhizome-associated alternative splicing and alternative polyadenylation in moso bamboo (*Phyllostachys edulis*), Plant J. 91 (4) (2017) 684–699, https://doi.org/10.1111/tpj.13597.

[30] C. Zhao, Y. Chen, Q. Lu, C. Shen, Evaluation on the superiorities of the ecological adaptability and pharmacodynamic actions of “purple Sanqi”, J. Yunnan Agric. Univ. 25 (4) (2010) 592–598, https://doi.org/10.16211/j.issn.1004-390x(n.

[31] C. Zhao, S. Yang, Z. Chen, et al., Contents of Total Anthocyanins and Total Saponins as Well as Composition of Saponin Monomers of Purple and Green Notoginseng Radix et Rhizoma, J. Chin. Med. Mater. 37 (10) (2014) 1749–1753, https://doi.org/10.13863/j.issn1001-4454.

[32] D. Yi, H. Zhang, B. Lai, et al., Integrative analysis of the coloring mechanism of red longan pericarp through metabolome and transcriptome analyses, J. Agric. Food Chem. 69 (6) (2021) 1806–1815, https://doi.org/10.1021/acs.jafc.0c05023.

[33] Z. Zhan, W. Fang, X. Ma, et al., Metabolome and transcriptome analyses reveal quality change in the orange-rooted *Salvia miltiorrhiza* (Danshen) from cultivated field, Chin. Med. 14 (2019) 42, https://doi.org/10.1186/s13020-019-0265-6.

[34] X. Sun, L. Li, J. Pei, C. Liu, L.F. Huang, Metabolome and transcriptome profiling reveals quality variation and underlying regulation of three ecotypes for *Cistanche deserticola*, Plant Mol. Biol. 102 (3) (2020) 253–269, https://doi.org/10.1007/s11103-019-00944-5.

[35] M. Kanehisa, S. Goto, KEGG: kyoto encyclopedia of genes and genomes, Nucleic Acids Res. 28 (1) (2000) 27–30, https://doi.org/10.1093/nar/28.1.27.

[36] M. Kanehisa, Toward understanding the origin and evolution of cellular organisms, Protein Sci. 28 (11) (2019) 1947–1951, https://doi.org/10.1002/pro.3715.

[37] M. Kanehisa, M. Furumichi, Y. Sato, M. Ishiguro-Watanabe, M. Tanabe, KEGG: integrating viruses and cellular organisms, Nucleic Acids Res. 49 (D1) (2021) D545–D551, https://doi.org/10.1093/nar/gkaa970.

[38] K. Cho, K.S. Cho, H.B. Sohn, et al., Network analysis of the metabolome and transcriptome reveals novel regulation of potato pigmentation, J. Exp. Bot. 67 (5) (2016) 1519–1533, https://doi.org/10.1093/jxb/erv549.

[39] G. Wei, F. Yang, F. Wei, et al., Metabolomes and transcriptomes revealed the saponin distribution in root tissues of *Panax quinquefolius* and *Panax notoginseng*, J. Ginseng Res. 44 (6) (2020) 757–769, https://doi.org/10.1016/j.jgr.2019.05.009.

[40] Z.S. Xu, Q.Q. Yang, K. Feng, A.S. Xiong, Changing carrot color: insertions in DcMYB7 alter the regulation of anthocyanin biosynthesis and modification, Plant Physiol 181 (1) (2019) 195–207, https://doi.org/10.1104/pp.19.00523.
[41] N. Ablat, D. Lv, R. Ren, et al., Neuroprotective effects of a standardized flavonoid extract from safflower against a rotenone-induced rat model of Parkinson's disease, Molecules 21 (9) (2016) 1107, https://doi.org/10.3390/molecules21091107.
[42] A.Y. Chen, Y.C. Chen, A review of the dietary flavonoid, kaempferol on human health and cancer chemoprevention, Food Chem. 138 (2013) 2099–2107, https://doi.org/10.1016/j.foodchem.2012.11.139.
[43] F. Wang, G. Ji, Z. Xu, et al., Metabolomics and transcriptomics provide insights into anthocyanin biosynthesis in the developing grains of purple wheat (*Triticum aestivum* L.), J. Agric. Food Chem. 69 (38) (2021) 11171–11184, https://doi.org/10.1021/acs.jafc.1c01719.
[44] S. Li, B. Deng, S. Tian, M. Guo, H. Liu, X. Zhao, Metabolic and transcriptomic analyses reveal different metabolite biosynthesis profiles between leaf buds and mature leaves in *Ziziphus jujuba* mill, Food Chem. 347 (2021) 129005, https://doi.org/10.1016/j.foodchem.2021.129005.
[45] A.A. Bennett, E.H. Mahood, K. Fan, G.D. Moghe, Untargeted metabolomics of purple and orange-fleshed sweet potatoes reveals a large structural diversity of anthocyanins and flavonoids, Sci. Rep. 11 (1) (2021) 16408, https://doi.org/10.1038/s41598-021-95901-y.
[46] J. Zhang, X. Qiu, Q. Tan, Q. Xiao, S. Mei, A comparative metabolomics study of flavonoids in radish with different skin and flesh colors (*Raphanus sativus* L.), J. Agric. Food Chem. 68 (49) (2020) 14463–14470, https://doi.org/10.1021/acs.jafc.0c05031.
[47] H. Zhou, K. Lin-Wang, F. Wang, et al., Activator-type R2R3-MYB genes induce a repressor-type R2R3-MYB gene to balance anthocyanin and proanthocyanidin accumulation, New Phytol. 221 (4) (2019) 1919–1934, https://doi.org/10.1111/nph.15486.
[48] A. Fatica, I. Bozzoni, Long non-coding RNAs: new players in cell differentiation and development, Nat. Rev. Genet. 15 (1) (2014) 7–21, https://doi.org/10.1038/nrg3606.
[49] X. Xue, Y. Duan, J. Wang, F. Ma, P. Li, Nighttime temperatures and sunlight intensities interact to influence anthocyanin biosynthesis and photooxidative sunburn in "fuji" apple, Front. Plant Sci. 12 (2021) 694954, https://doi.org/10.3389/fpls.2021.694954.